JTTEE5 19:602–610
DOI: 10.1007/s11666-009-9460-9
1059-9630/$19.00 © ASM International

Splat Morphology of Yttria-Stabilized Zirconia Droplet Deposited Via Hybrid Plasma Spraying

Kentaro Shinoda and Hideyuki Murakami

(Submitted May 15, 2009; in revised form October 2, 2009)

The splat morphology of yttria-stabilized zirconia (YSZ) droplets deposited by dc-rf hybrid plasma spraying (HYPS) was studied. Two types of YSZ powder were used, namely fused and crushed powder (FC) and hollow spherical powder (HOSP). The three-dimensional shape of more than 600 disk-shaped splats on preheated substrates was evaluated using a laser-scanning microscope to determine the splat diameter, thickness, and their dimensionless forms. The HOSP showed a higher degree of flattening than the FC. Both the FC with a powder size distribution of 45-75 μm and the HOSP of 30-120 μm can be used as spray materials in the HYPS to achieve a coating design based on fully molten particles. The effect of the substrate temperature on the splat morphology was similar to that of atmospheric dc plasma spraying; however, the transition from a splashed shape to a disk shape gradually occurred at higher substrate temperatures.

Keywords diagnostics and control, preheating of substrate, RF induction plasma spraying, TBC topcoats

1. Introduction

A dc-rf hybrid plasma has been applied to the plasma spraying technique, called hybrid plasma spraying (HYPS) (Ref 1-4). The residence time of particles in the hybrid plasma jet is one order of magnitude longer and the plasma jet diameter is also five to ten times larger than those of the atmospheric dc plasma jet. These characteristics enable the HYPS to completely melt the injected powder particles. For example, a melting index, which was proposed to express the melting state of particles by Xiong et al. (Ref 5) and given by the ratio of the residence time of a particle to the time required for the particle to be fully melted, can be ten times greater. Thus, the design of coatings based on fully molten particles is available by the HYPS, and a dense electrolyte for solid oxide fuel cells was actually produced by this method (Ref 2, 6, 7). This melting capability also enables the vaporization of fine powder less than 10 μm, which has been used for thermal plasma physical vapor deposition (Ref 8, 9). A new plasma spray process combining these two techniques is a promising candidate to produce next generation thermal barrier coatings (Ref 4, 10, 11).

Kentaro Shinoda and **Hideyuki Murakami**, Hybrid Materials Center, National Institute for Materials Science (NIMS), 1-2-1 Sengen, Tsukuba, Ibaraki 305-0047, Japan. Contact e-mail: shinoda.kentaro@nims.go.jp.

Coating architecture based on fully molten particles requires an understanding of the splat morphology of the HYPS. However, the splat morphology of the HYPS has not been systematically studied when compared to that of the APS (Ref 12-18). Powder morphology is the first concern. In the case of the APS, fused and crushed powder (FC) and hollow spherical powder (HOSP) are often used as spray materials. The FC is used to obtain a dense coating, and the HOSP produces a porous coating (Ref 19, 20). In contrast to the APS, the HYPS coating architecture is based on complete melting of the injected powder particles. Therefore, the powder morphology effect should be reconsidered. The melting capability of each powder is also important. It is obvious that the HYPS can melt larger size powder than the APS, yet one needs to know how large powder can be actually sprayed for these two types of powder.

The effect of the substrate temperature on the splat morphology is another issue to be investigated. It is well known that the splat takes on a splashed shape below a certain substrate temperature called the transition temperature in the APS and exhibits a disk shape above the transition temperature (Ref 21, 22). The splashing of splats may reduce the deposition efficiency, cause poor adhesion of the splats, and reduce the coating quality. Thus, it is important to understand the transition phenomena of splats. Many phenomena, such as the particle impact energy (Ref 23), poor wettability (Ref 24), surface adsorbate (Ref 25), surface oxidation of a substrate (Ref 26), rapid solidification of a spreading droplet (Ref 27), and surrounding pressure (Ref 28), can cause the splashing of splats. The impacting speed of particles in the HYPS is typically 30-70 m/s and much slower than that of the APS (100-300 m/s). Therefore, the transition behavior of the HYPS may be different from that of the APS.

The objective of this paper is to study the morphology of YSZ splats deposited by the HYPS. Two kinds of powder, that is, FC and HOSP, were examined over a wide range of powder sizes. The effect of the substrate temperature on the splat morphology was also examined. The feasibility of the HYPS was discussed using a previously reported model (Ref 15).

2. Experimental

Figure 1 shows the schematic diagram of the experimental apparatus, which consists of a 4 MHz-50 kW rf power supply, a 10 kW dc power supply, a dc-rf hybrid plasma torch, an airtight chamber, a powder feeder, a gas-feeding system, a water-cooling system, and a vacuum system. Detailed description of the HYPS system is described elsewhere (Ref 1, 6, 16).

Two types of YSZ powder were used in this study: one was conventional FC, which was the same composition as K-90 (Showa Denko K.K., Tokyo, Japan) but had a larger size distribution that was sieved into two nominal diameter ranges; that is, small (S) 37-44 μm and medium (M) 63-88 μm. The other was HOSP (204C-NS, Sulzer Metco, USA) into three ranges; that is, small (S) 37-44 μm, medium (M) 63-74 μm, and large (L) 88-125 μm. The purpose of the powder sieving is to easily observe the splat morphology as a function of a droplet diameter. These types of powder were sprayed by an argon-hydrogen atmospheric plasma under the conditions shown in Table 1(a). The distance between the torch exit and the substrate was fixed at 70 mm. A boron nitride (BN) plate with a 1 mm diameter orifice was mounted 30 mm above a substrate to reduce the number of particles reaching the substrate. This cover also plays an important role in controlling the substrate temperature to prevent the substrate from direct heating by the plasma jet and to heat the substrate gradually by its radiation. Mirror-polished stainless steel plates (AISI 304, 50 × 50 × 6 mm) and smooth quartz glass plates (50 × 50 × 0.5 mm) were used as the substrates. The substrates were rotated during the experiments to avoid any overlap of the splats and pre-heated with the BN plate prior to the splat deposition. The substrate temperature, T_s, was measured at the bottom side of the substrate with a K-type thermocouple. Figure 2 shows a typical temperature history of a stainless steel substrate. The value of T_s gradually increased during the pre-heating from 303 to 763 K within 180 s. It should be noted that no substrate oxidation occurred, because the experiments were conducted in an argon-hydrogen atmosphere in the airtight chamber.

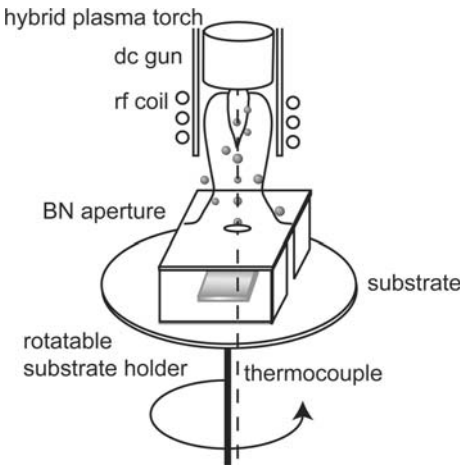

Fig. 1 Schematic diagram of experimental setup to collect single splats. The system is built inside an airtight chamber

The splat morphology in a three-dimensional shape was measured with a laser-scanning microscope (LSM) (Model VK-8500, Keyence Corp., Osaka, Japan). Moreover, in the case of the quartz glass substrates, the splats were observed from the bottom side through the substrate. The splat morphology of more than 600 disk-shaped splats on the stainless steel substrates obtained at $T_s = 763$ K, which was considered to be well above the transition temperature, was evaluated to determine the effect of the powder particle size. Here, the particle diameter d was derived from the splat volume, which could be measured with the LSM. Therefore, the value of d corresponds to the diameter of a fully molten non-hollow solid droplet before impact. It should be noted that d should be smaller than the initial powder diameter in the case of the HOSP. The splat diameter D was defined by the average of the splat diameters in two orthogonal directions. The splat thickness Z was derived from the splat volume and D, assuming that the splat had a flat circular disc shape. The dimensionless forms of D and Z with respect to d were also derived to evaluate the droplet deposit dynamics, i.e., the degree of flattening, ξ, which was defined by $\xi = D/d$; and the other was the degree of flattening in thickness, ζ, defined by $\zeta = Z/d$.

During the HYPS, some splats showed a unique shape and morphology, which differed from those obtained by the conventional APS. These splats were also examined by scanning electron microscopy (SEM), energy-disperse x-ray spectrometry (SEM-EDS), and electron probe wavelength-disperse x-ray spectrometry (EPMA).

To examine the effect of T_s, the change in the splat morphology was carefully observed at the five points indicated in Fig. 2, i.e., $T_s = 303$, 408, 513, 673, and 763 K.

Table 1 Plasma conditions

Operating parameters	(a) HYPS	(b) APS
dc plasma torch		
Ar gas flow rate, SLM*	10	50
He gas flow rate, SLM		13
dc current, A	400	800
rf plasma torch		
Radial Ar gas flow rate, SLM	30	
Tangential Ar gas flow rate, SLM	20	
Radial H_2 gas flow rate, SLM	5	
Input power, kW	50	

*Standard liters per minute

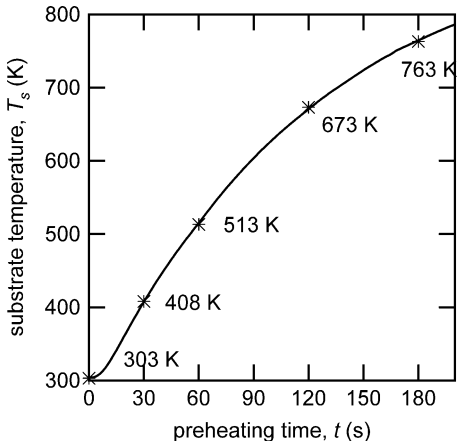

Fig. 2 Substrate temperature T_s as a function of preheating time t. The splats were collected at the five temperatures shown in the figure

For the purpose of comparison, splats were also collected by APS. To collect the splats, the FC of 8 wt.% YSZ (K-90, Showa Denko K.K., Tokyo, Japan) with the nominal diameter of 10-44 μm were sprayed by a conventional dc plasma torch with a 40 kW subsonic anode (SG-100 with type 2083-165 anode, TAFA, Inc., A Praxair Surface Technologies, Inc., NH, USA). Only one kind of powder (i.e. FC) was examined because the process difference between HYPS and APS would be much larger than the powder morphology difference between HOSP and FC in APS. A 25-kW argon-helium plasma was used as shown in Table 1(b). A stainless steel (AISI 304) substrate with the thickness of 5 mm was used, and the substrate temperature was kept at 500 K, which was measured at a position 2.5 mm from the substrate surface with a K-type thermocouple. The stand-off distance was 100 mm.

3. Results

Almost all the splats of the FC and the HOSP deposited on a stainless steel substrate at $T_s = 763$ K by the HYPS were disk-shaped, while some HOSP splats of $d > 80$ μm and FC splats of $d > 75$ μm had unmolten cores or shells, indicating that both the HOSP and the FC up to roughly $d = 75$ μm can be completely melted by the HYPS. Many tiny droplets (approximately a few microns) were deposited on substrates in the case of the HOSP. The values of D and Z of those splats are plotted as a function of d in Fig. 3(a) and (b), respectively. Those of the APS are also shown in Fig. 3 for comparison. The HOSP had a larger D than the FC and the difference in D became greater with the increasing d. The value of D of the HOSP was nearly 300 μm at $d = 75$ μm. Interesting findings were that Z was almost constant over the wide range of d ($25 < d < 60$ μm), while D monotonically increased over d. The values of Z of the HOSP and the FC were approximately 2 and 3 μm, respectively. This was in

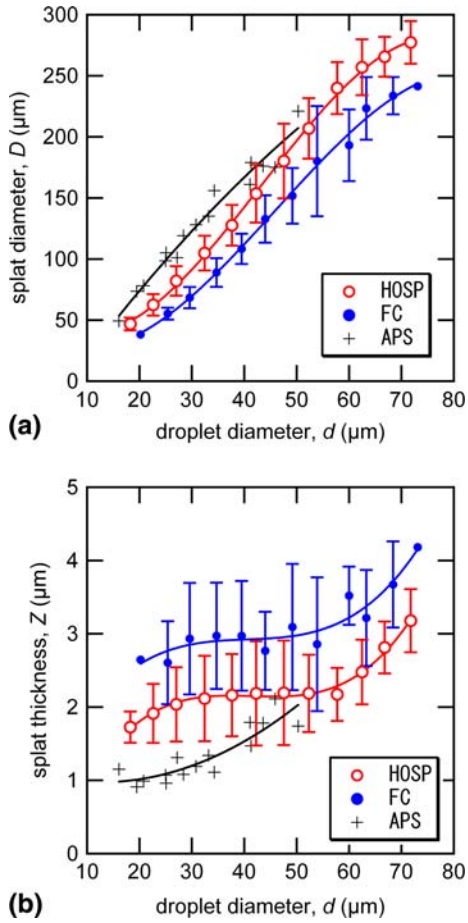

Fig. 3 (Color online) Dependence of (a) splat diameter D and (b) splat thickness Z on droplet diameter d for hollow spherical powder (HOSP) and fused and crushed powder (FC) deposited by hybrid plasma spraying. The values of D and Z were averaged for every 5 μm of d. The points of FC are offset 2 μm to right. The values of D and Z of the FC deposited by atmospheric dc plasma spraying (APS) are also shown for comparison. The error bars indicate a standard deviation. Since the number of data points of the APS was not enough, all the data points are shown instead of average values with error bars in the case of the APS

contrast to Z of the APS, which monotonically increased from 1 to 2 μm as a function of d. The value of Z of the HOSP was 1 μm less than that of the FC over the range of d.

Figure 4(a) and (b) shows ξ and ζ versus d, respectively. The HOSP had roughly a 0.5 higher ξ than the FC for all the d. At $50 < d < 70$ μm, the HOSP showed $\xi = 4$, which was comparable to the APS. In contrast to Fig. 3(b), the values of ζ of the HYPS monotonically decreased with the increasing d up to 50 μm, while that of the APS decreased and then increased with the increasing d, even though the magnitude of the change was smaller than that of the HYPS. Both types of powder had peaks of ξ at a similar location around $55 < d < 65$ μm. This change can also be seen in Fig. 3(a), (b) and 4(b) as a change in the gradient. Taking into account the fact that splats with $d > 75$ μm had unmolten cores or shells, it is rational that the particle temperature tended to decrease

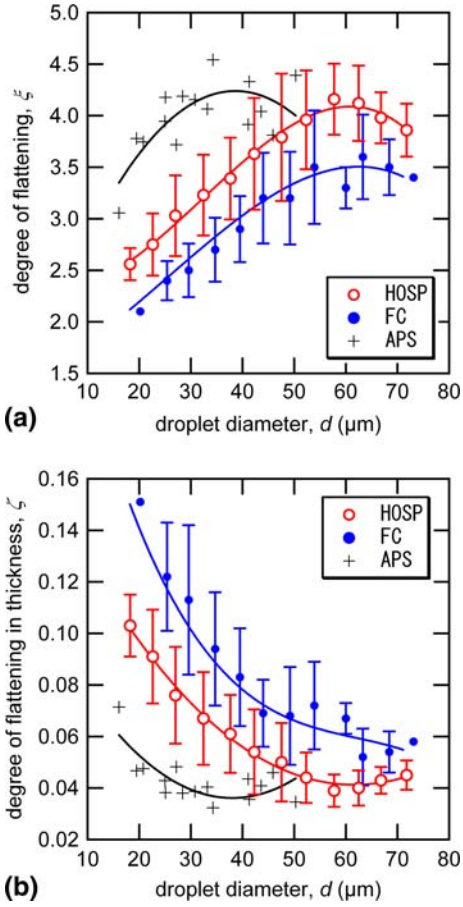

Fig. 4 (Color online) The dependence of (a) the degree of flattening, ξ, and (b) the degree of flattening in thickness, ζ, on the droplet diameter d for hollow spherical powder (HOSP) and fused and crushed powder (FC) deposited by hybrid plasma spraying. The values of ξ and ζ were averaged for every 5 μm of d. The points of FC are offset 2 μm to right. The values of ξ and ζ of the FC deposited by atmospheric dc plasma spraying (APS) are also shown for comparison. The error bars indicate a standard deviation. Since the number of data points of the APS was not enough, all the data points are shown instead of average values with error bars in the case of the APS

above $d = 60$ μm, and particles were not fully molten above $d = 75$ μm.

Figure 5 summarizes the morphological changes in the splats as a function of ξ ($2 \le \xi \le 5$). These top and lateral images indicate drastic change in the splat morphology. At lower ξ (~2), the splat exhibited a dome-like shape in which the central region was thicker than the periphery. For higher ξ (≥3), the splat morphology was similar to that of the APS; that is, the splat had a smooth surface with a rounded rim. The size of the rim was greater than that of the APS. When the thickness of a splat was thinner ($Z < 1.5$ μm), the substrate surface could be observed through the splat.

Among these splats, the splats with ξ ~ 2 were further investigated. In order to characterize the particle impact kinetics, a similar splat was extracted from an experimental database in our previous study, which was a similar condition to this study (Ref 15). Figure 6 shows secondary electron images of the surface morphology and microstructure of a splat with $\xi = 2.0$. In situ measurements revealed that this splat was formed from a droplet of $d = 47$ μm impacting at 2712 K (undercooled state) and at a speed of 16 m/s, which was lower than the typical impact speed in the HYPS (30-70 m/s). The surface of the splat showed a peculiar structure (Fig. 6b), which was different from the conventional columnar microstructure that was observed in a splat with $\xi > 3$ (an example is given in Fig. 6c). The dendrite-like microstructure shown in Fig. 6(b) implied the non-facet growth of the YSZ. Both SEM-EDS and EPMA confirmed that these splats had the same composition as the powder materials. Therefore, the formation of a dendritic structure was not attributed to the composition change but probably to a lower impact velocity and/or the undercooling of the droplet.

Finally, Fig. 7 and 8, respectively, show the typical splat morphology of the FC and that of the HOSP deposited onto quartz glass substrates at T_s ranging from room temperature to 763 K. There were no distinct differences in the splat shapes between the FC and the HOSP. The splats of both types of powder gradually changed their shape from a splashed one to a disk-shaped one as T_s increased. The transition temperatures were between 513 and 673 K. Although it was not statistically confirmed, the small splats ($D < 100$ μm) tended to show a disk-shape, while the larger splats ($D > 250$ μm) sometimes exhibited a disk shape but with fingers even at the higher T_s. Although the splat shapes were similar between the HOSP and the FC, crack patterns were different; the crack patterns in the radial directions were more apparent for the FC splats than that for the HOSP.

4. Discussion

4.1 Morphology of YSZ Splats

The morphology of disk-shaped splats deposited by the HYPS was evaluated through four indices as a function of the particle diameter d; that is, the splat diameter D, the splat thickness Z, and their dimensionless forms (i.e., the degree of flattening), ξ and ζ, respectively. We now discuss how the splat morphology of the HYPS differs from that of the APS with the help of a simple analytical model.

When neglecting the contribution of the splat rim on the splat morphology, an analytical model developed by Pasandideh-Fard et al. (Ref 29) well describes the splat morphology (Ref 15). When a droplet with the diameter d and kinematic viscosity ν impinges on a substrate at a speed V, the degree of flattening, ξ, is given by (Ref 29):

$$\xi = \frac{D}{d} = \frac{1}{2}\left(\frac{Vd}{\nu}\right)^{1/4} \quad \text{(Eq 1)}$$

The actual splat diameter D can be thus predicted by

$$D = \frac{1}{2}\frac{V^{1/4}d^{5/4}}{\nu^{1/4}} \quad \text{(Eq 2)}$$

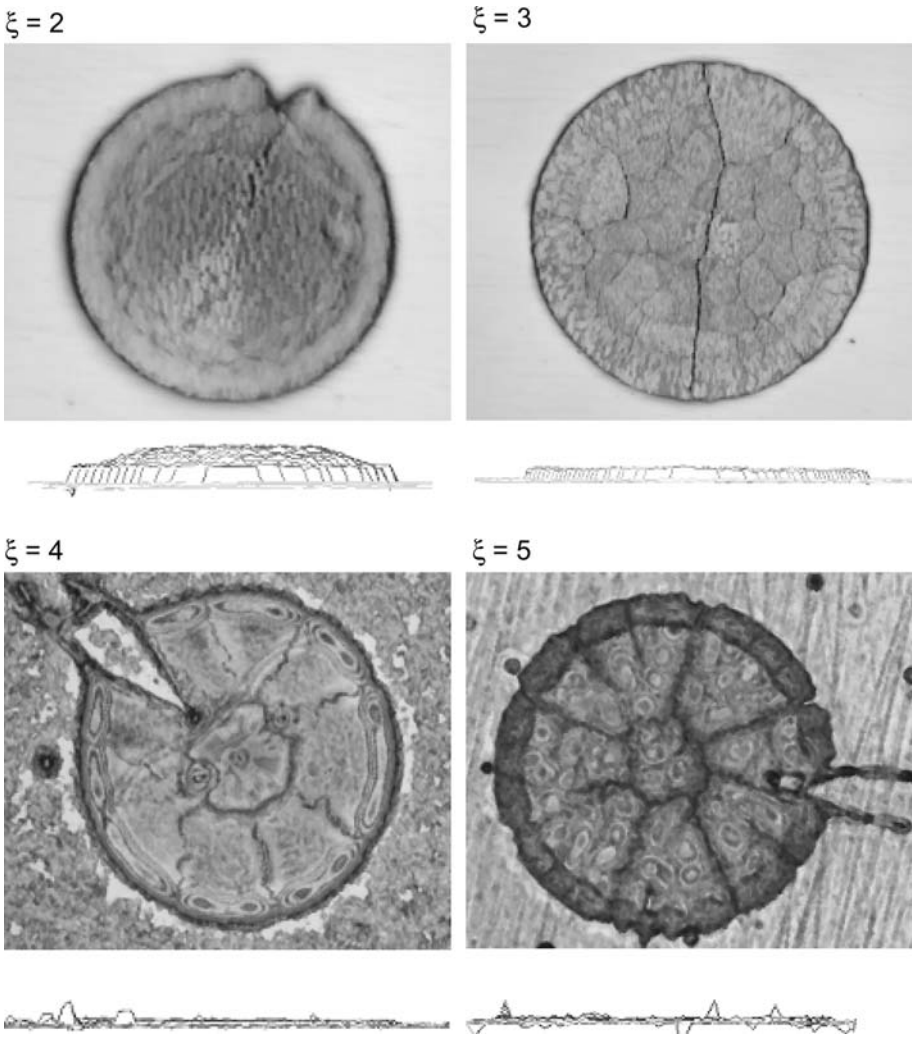

Fig. 5 Laser-scanning microscope images of splat morphologies from top and lateral views for various degrees of flattening, ξ. The splats with $\xi = 2, 3$ and with $\xi = 4, 5$ were deposited from fused and crushed powder and hollow spherical powder, respectively

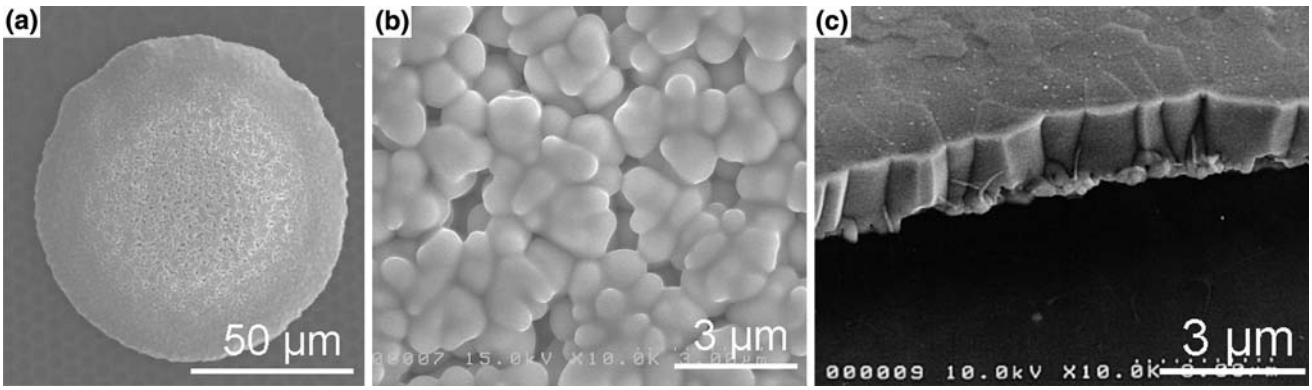

Fig. 6 Secondary electron images of splat morphology whose degree of flattening is 2.0. (a) Whole image. (b) Magnified view of center part. This droplet had a 47 μm diameter and impinged on a substrate at the speed of 16 m/s and the temperature of 2712 K. (c) Fracture surface of a typical splat that has a columnar structure

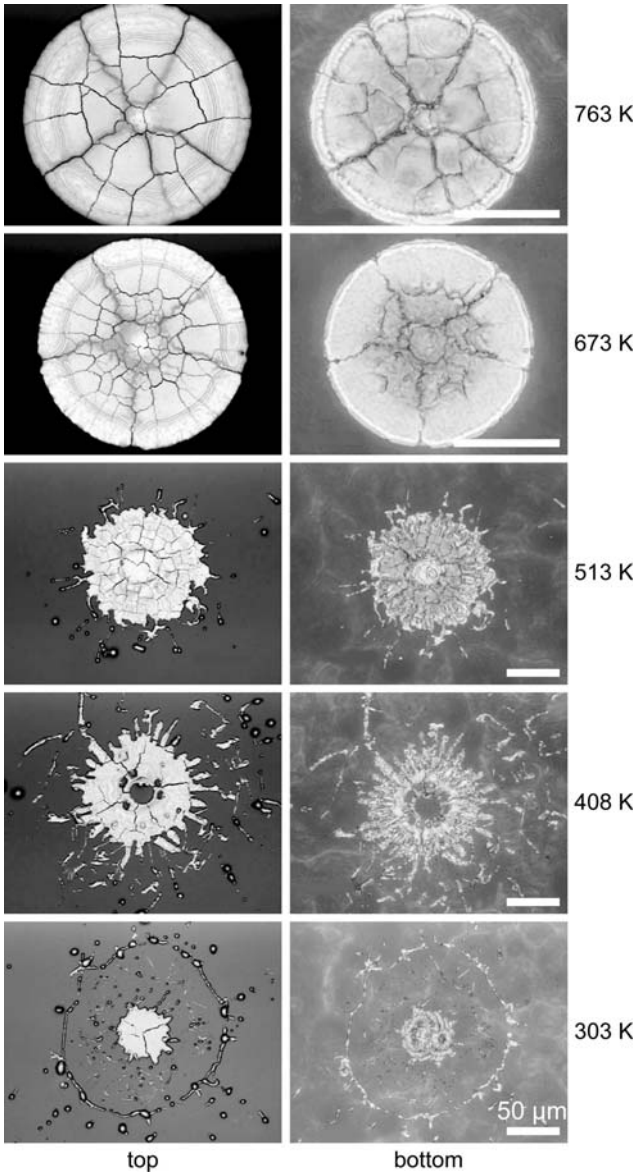

Fig. 7 Laser-scanning microscope images of top side (left) and bottom side (right) of YSZ splats of fused and crushed powder deposited onto quartz glass substrate at various substrate temperatures. The images of the backsides of the splats appear as a reflection flipped left-to-right so that the correspondence between the top and bottom surface is easy. Bar indicates 50 μm

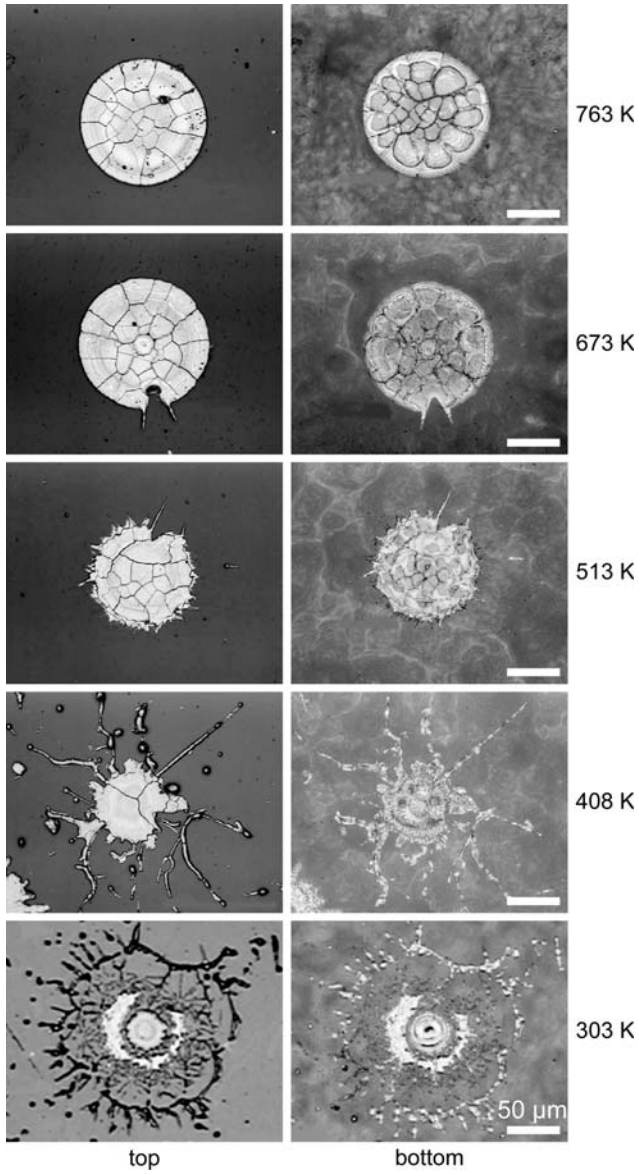

Fig. 8 Laser-scanning microscope images of top side (left) and bottom side (right) of YSZ splats of hollow spherical powder deposited onto quartz glass substrate at various substrate temperatures. The images of the backsides of the splats appear as a reflection flipped left-to-right so that the correspondence between the top and bottom surface is easy. Bar indicates 50 μm

Equation 2 clearly shows that the initial droplet diameter d is the primary factor that determines the splat diameter D. In the case of the APS, since the maximum size of the particles is limited due to the melting capability, the primary strategy to increase d is not practical. On the contrary, HYPS can use this strategy thanks to its high melting capability. Thus, as shown in Fig. 3(a), large splats up to 300 μm can be obtained by the HYPS, even though the impact speeds of the particles were at most 30-70 m/s.

Assuming that a splat has a cylindrical shape, the dimensionless splat thickness ζ can be derived from Eq 1 as

$$\zeta = \frac{Z}{d} = \frac{8}{3}\left(\frac{\nu}{Vd}\right)^{1/2} \quad \text{(Eq 3)}$$

Therefore, the actual splat thickness Z can be given by

$$Z = \frac{8}{3}\left(\frac{\nu d}{V}\right)^{1/2} \quad \text{(Eq 4)}$$

In Fig. 4, the value of ξ turned to decrease and ζ to increase above a certain diameter d_c for both the APS and

the HYPS. According to Eq 1 and 3, this implies that a drop of V/ν was much bigger than the increase of d above d_c; that is, the drop of particle velocity and/or temperature cannot be negligible above a certain particle diameter, because ν has an inverse relationship with the particle temperature. Moreover, d_c of the APS was smaller than that of the HYPS, suggesting that the drop of particle velocity and/or temperature occurs at a smaller diameter in the APS compared to the HYPS.

However, when converting ζ into a real thickness Z, an interesting phenomenon happens; as shown in Fig. 3(b), the value of Z of the HYPS was almost constant over the wide range of $d < 60$ μm despite that ζ decreased with the increasing d, which is in contrast to that of the APS, which monotonically increased. This means that $\nu d/V$ can be almost constant in the HYPS, while it increased monotonically with the increasing d in the APS according to Eq 4. Although further investigation is needed to confirm this phenomenon, a relationship between particle size and velocity may partly explain this. A simulation done by Xiong et al. (Ref 30) showed that larger particles tend to have higher velocity in rf induction plasma spraying, which is in contrast to the APS in which larger particles tend to have lower velocity (Ref 5, 31). If the particle acceleration mechanism of the HYPS can be regarded as a similar mechanism to the rf induction plasma spraying, the value of $\nu d/V$ may be constant in the HYPS, while that of the APS may increase, within a range where temperature drop is not so large compared to the diameter change.

The uniform thickness of the splats over the wide range of d (<60 μm) may be useful to design a uniform microstructure coating. For example, as was summarized by Huang et al. (Ref 9), the next generation TBCs require a layering structure to prevent thermal radiation transfer, which becomes significant at high temperatures over 1473 K (Ref 32). The uniform thickness of the splats can be helpful when designing such a coating.

It is noteworthy that the splat morphology could be explained with a help of an analytical model. This means that the in-flight state of particles can be estimated to some extent from an ex situ observation of the splat morphology. Thermal spray systems in an airtight chamber, such as the HYPS system and a low pressure plasma spray system, are often difficult to do in-flight diagnostics. In such a case, the splat morphology evaluation as a function of d will be a strong tool.

4.2 Effect of Powder Morphology: HOSP and FC

The degrees of flattening, ξ, of the HOSP were always greater than those of the FC. According to Eq 1, this means that V/ν of the HOSP must always be greater than that of the FC. That is, both the temperatures and velocities of the HOSP particles were expected to be higher than those of the FC. This was the same tendency as the APS (Ref 20).

This tendency can be explained by considering the actual outer diameter of an injected HOSP particle. In this study, we described the size of a single powder particle by the equivalent volume sphere diameter d. Thus, even for the same d, the initial diameter of the HOSP particle was larger than that of the FC. Therefore, until the HOSP particle was completely melted and formed a full-filled molten droplet, the HOSP particle had a larger diameter and a larger surface to mass ratio than the FC. Since this apparent larger diameter gives a larger drag force, the HOSP particle was expected to be accelerated more and to have a higher speed than the FC. The large surface to mass ratio increases the heat transfer from the plasmas, and the HOSP particle could have a higher temperature than the FC. Thus, as well as the APS, the HOSP particles had higher temperatures and velocities than the FC.

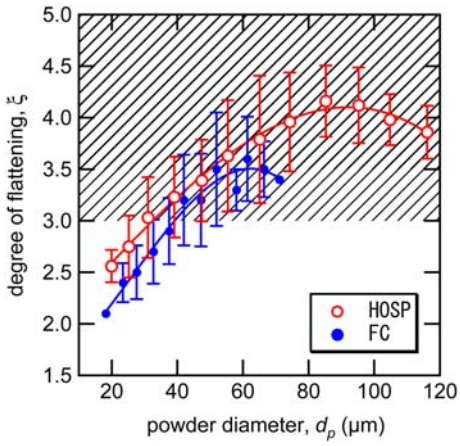

Fig. 9 (Color online) The dependence of the degree of flattening, ξ, on the initial powder diameter d_p for hollow spherical powder (HOSP) and fused and crushed powder (FC) in the hybrid plasma spraying. The region where the degree of flattening, $\xi \geq 3$ is hatched

The actual initial powder diameter d_p before molten should be greater than d for the HOSP. The value of d_p of the HOSP can be estimated by assuming that the shell thickness of the HOSP particle is 10 μm (Ref 33). Figure 9 re-plotted Fig. 4(a) as a function of d_p. To fill the gap between a single splat test and an actual coating, Hamatani et al. (Ref 6) reported an empirical rule in which a dense coating was obtained at $\xi > 3$ in the HYPS. By adding this criterion to Fig. 9, we can see the wide range of powder sizes of the FC and HOSP that are suitable for the HYPS; that is, the FC with the size $40 < d_p < 75$ μm and the HOSP with the size $30 < d_p < 120$ μm can be used in the HYPS. These values were much greater than the full-melting limitation of the APS, which were calculated to be $d_p = 50$ μm and 60-90 μm for the FC and the HOSP, respectively (Ref 33).

4.3 Effect of Substrate Temperature on Splat Morphology

The transition of the splat morphology when the substrate temperature changes is a well-known phenomenon in the APS. This study showed that this transition also occurred in the HYPS. The morphology of a splat splashing on a room temperature substrate in this study was similar to the splashing images of the one impacting

on a room temperature substrate in the APS (Ref 12). Thus, the splashing of the splat in the HYPS probably occurs by the same mechanism as the APS. That is, the transition phenomena of YSZ splats occur for a wide range of impact velocities ($30 < V < 200$ m/s).

Although the splat morphology was similar to that of the APS, the transition temperature was higher than that of the APS. The transition occurs at $513 < T_s < 673$ K for the HYPS, while at $T_s < 500$ K for the APS (Ref 28). An increase in the transition temperature with the increasing impact velocity was also reported in the case of aluminum wire arc spraying, which can be explained by the thickness change of the initial solidification layer (Ref 34). However, as Dhiman et al. reported (Ref 35), the effect of solidification on inducing splashing is rather small in the case of YSZ. Taking into account the fact that smaller particles tended to exhibit a disk shape even at a low T_s, the transition temperature may slightly depend on the particle size and velocity themselves. These similarities and differences in the transition behavior do not directly show the feasibility of the HYPS, yet they can be a guide for the development of the HYPS.

5. Conclusions

More than 600 YSZ splats deposited by the HYPS were observed with the LSM. The morphology of the splats was evaluated with the help of an analytical model and compared to the APS. The HOSP showed the greater degree of flattening than the FC. Both the FC with a powder size distribution of 45-75 μm and the HOSP of 30-120 μm can be used as spray materials in the HYPS to achieve a coating design based on fully molten particles. Interesting findings were that the splat thickness was almost the same over a wide range of particle sizes, which may help to obtain a uniform coating. The effect of the substrate temperature on the splat morphology was similar to that of the APS; however, the transition from a splashed shape to a disk shape gradually occurred, and the transition temperature was higher than that of the APS.

Acknowledgments

The HYPS experiment was conducted at the University of Tokyo. The authors express their deep gratitude to Dr. Peng Han (the University of Tokyo) for his assistance in the experiment and also to Prof. Toyonobu Yoshida (the University of Tokyo) for the useful discussions.

References

1. T. Yoshida, T. Tani, H. Nishimura, and K. Akashi, Characterization of a Hybrid Plasma and Its Application to Chemical Synthesis, *J. Appl. Phys.*, 1983, **54**(2), p 640-646
2. H. Hamatani, H. Kumaoka, T. Yahata, and T. Yoshida, An Integrated Fabrication Process for Solid Oxide Fuel-Cells Using Hybrid Plasma Spraying, *J. Jpn. Inst. Met.*, 1991, **55**(11), p 1240-1248
3. T. Yoshida, The Future of Thermal Plasma Processing, *Mater. Trans. JIM*, 1990, **31**(1), p 1-11
4. H. Huang, K. Eguchi, and T. Yoshida, High-Power Hybrid Plasma Spraying of Large Yttria-Stabilized Zirconia Powder, *J. Therm. Spray Technol.*, 2006, **15**(1), p 72-82
5. H.B. Xiong, L.L. Zheng, L. Li, and A. Vaidya, Melting and Oxidation Behavior of In-Flight Particles in Plasma Spray Process, *Int. J. Heat Mass Transf.*, 2005, **48**(25-26), p 5121-5133
6. T. Yoshida, T. Okada, H. Hamatani, and H. Kumaoka, Integrated Fabrication Process for Solid Oxide Fuel Cells Using Novel Plasma Spraying, *Plasma Sources Sci. Technol.*, 1992, **1**(3), p 195-201
7. N. Nomoto, Y. Okazaki, K. Kuroda, S. Takenoiri, and T. Yoshida, Integrated Fabrication Process for Solid Oxide Fuel Cells Using Hybrid Plasma Spraying, *High Temp. Mater. Process.*, 1997, **1**(1), p 41-48
8. J.Q. Li, H.J. Huang, T. Ma, K. Eguchi, and T. Yoshida, Twin-Structured Yttria-Stabilized T′ Zirconia Coatings Deposited by Plasma Spray Physical Vapor Deposition: Microstructure and Mechanical Properties, *J. Am. Ceram. Soc.*, 2007, **90**(2), p 603-607
9. H. Huang, K. Eguchi, M. Kambara, and T. Yoshida, Ultrafast Thermal Plasma Physical Vapor Deposition of Yttria-Stabilized Zirconia for Novel Thermal Barrier Coatings, *J. Therm. Spray Technol.*, 2006, **15**(1), p 83-91
10. H. Huang, K. Eguchi, and T. Yoshida, Novel Structured Yttria-Stabilized Zirconia Coatings Fabricated by Hybrid Thermal Plasma Spraying, *Sci. Technol. Adv. Mater.*, 2003, **4**(6), p 617-622
11. K. Eguchi, H. Huang, M. Kambara, and T. Yoshida, Twin Hybrid Plasma Spray Deposition of Novel Thermal Barrier YSZ Composite Coatings, *J. Jpn. Inst. Met.*, 2005, **69**(1), p 17-22
12. K. Shinoda, H. Murakami, S. Kuroda, S. Oki, K. Takehara, and T.G. Etoh, High-Speed Thermal Imaging of Yttria-Stabilized Zirconia Droplet Impinging on Substrate in Plasma Spraying, *Appl. Phys. Lett.*, 2007, **90**(19), Art. No. 194103 (3 pages)
13. O.P. Solonenko, M.A. Anatol'yevich, K.E. Vladimirovich, B.M. Petrovna, K. Ogawa, T. Shoji, and M. Tanno, Theoretical Modeling and Experimental Study of Thermal Barrier Coatings, *Mater. Trans.*, 2003, **44**(11), p 2311-2321
14. K. Shinoda, A. Yamada, M. Kambara, Y. Kojima, and T. Yoshida, Deformation of Alumina Droplets on Micro-Patterned Substrates Under Plasma Spraying Conditions, *J. Therm. Spray Technol.*, 2007, **16**(2), p 300-305
15. K. Shinoda, T. Koseki, and T. Yoshida, Influence of Impact Parameters of Zirconia Droplets on Splat Formation and Morphology in Plasma Spraying, *J. Appl. Phys.*, 2006, **100**(7), Art. No. 074903 (6 pages)
16. K. Shinoda, Y. Kojima, and T. Yoshida, In Situ Measurement System for Deformation and Solidification Phenomena of Yttria-Stabilized Zirconia Droplets Impinging on Quartz Glass Substrate Under Plasma Spraying Conditions, *J. Therm. Spray Technol.*, 2005, **14**(4), p 511-517
17. Y.K. Chae, J. Mostaghimi, and T. Yoshida, Deformation and Solidification Process of a Super-Cooled Droplet Impacting on the Substrate Under Plasma Spraying Conditions, *Sci. Technol. Adv. Mater.*, 2000, **1**(3), p 147-156
18. K. Shinoda, M. Raessi, J. Mostaghimi, T. Yoshida, and H. Murakami, Effect of Concave Pattern of Substrate on Splat Formation of Yttria-Stabilized Zirconia in Atmospheric Plasma Spraying, *J. Therm. Spray Technol.*, 2009, **18**(4), p 609-618
19. Z. Wang, A. Kulkarni, S. Deshpande, T. Nakamura, and H. Herman, Effects of Pores and Interfaces on Effective Properties of Plasma Sprayed Zirconia Coatings, *Acta Mater.*, 2003, **51**(18), p 5319-5334
20. H.B. Guo, S. Kuroda, and H. Murakami, Microstructures and Properties of Plasma-Sprayed Segmented Thermal Barrier Coatings, *J. Am. Ceram. Soc.*, 2006, **89**(4), p 1432-1439
21. E.C. Rollason, T.H. Turner, and N.F. Budgen, *Metal Spraying*, 2nd ed., Charles Griffin & Co., Ltd., London, 1939, p 235
22. P. Fauchais, M. Fukumoto, A. Vardelle, and M. Vardelle, Knowledge Concerning Splat Formation: An Invited Review, *J. Therm. Spray Technol.*, 2004, **13**(3), p 337-360

23. C. Escure, M. Vardelle, and P. Fauchais, Experimental and Theoretical Study of the Impact of Alumina Droplets on Cold and Hot Substrates, *Plasma. Chem. Plasma Process.*, 2003, **23**(2), p 185-221
24. M. Fukumoto and Y. Huang, Flattening Mechanism in Thermal Sprayed Nickel Particle Impinging on Flat Substrate Surface, *J. Therm. Spray Technol.*, 1999, **8**(3), p 427-432
25. X.Y. Jiang, Y.P. Wan, H. Herman, and S. Sampath, Role of Condensates and Adsorbates on Substrate Surface on Fragmentation of Impinging Molten Droplets During Thermal Spray, *Thin Solid Films*, 2001, **385**(1-2), p 132-141
26. M. Fukumoto, M. Ohgitani, and T. Yasui, Effect of Substrate Surface Change on Flattening Behaviour of Thermal Sprayed Particles, *Mater. Trans.*, 2004, **45**(6), p 1869-1873
27. R. Dhiman and S. Chandra, Freezing-Induced Splashing During Impact of Molten Metal Droplets with High Weber Numbers, *Int. J. Heat Mass Transf.*, 2005, **48**(25-26), p 5625-5638
28. M. Fukumoto, M. Shiiba, H. Kaji, and T. Yasui, Three-Dimensional Transition Map of Flattening Behavior in the Thermal Spray Process, *Pure Appl. Chem.*, 2005, **77**(2), p 429-442
29. M. Pasandideh Fard, Y.M. Qiao, S. Chandra, and J. Mostaghimi, Capillary Effects During Droplet Impact on a Solid Surface, *Phys. Fluids*, 1996, **8**(3), p 650-659
30. H.B. Xiong, L.L. Zheng, M.Y. Zhang, H. Zhang, J. Margolies, and S. Sampath, Numerical Study of Particle in-Flight Characteristics in a RF Induction Plasma Spray, *Proceedings of the International Thermal Spray Conference 2005*, E. Lugscheider, Ed. (Basil, Switzerland), DVS, Germany, 2005, p 1349-1355
31. B.M. Cetegen and W. Yu, In-Situ Particle Temperature, Velocity, and Size Measurements in DC Arc Plasma Thermal Sprays, *J. Therm. Spray Technol.*, 1999, **8**(1), p 57-67
32. J.R. Nicholls, K.J. Lawson, A. Johnstone, and D.S. Rickerby, Methods to Reduce the Thermal Conductivity of Eb-Pvd Tbcs, *Surf. Coat. Technol.*, 2002, **151**, p 383-391
33. T. Clocker, T.W. Clyne, and M.R. Dorfman, Process Modelling to Optimize the Structure of Hollow Zirconia Particles for Use in Plasma Sprayed Thermal Barrier Coatings, *Thermal Spray 2001: New Surfaces for a New Millennium*, C.C. Berndt, K.A. Khor, and E.F. Lugscheider, Ed., May 28-30, 2001 (Singapore), ASM International, 2001, p 149-155
34. A. Abedini, A. Pourmousa, S. Chandra, and J. Mostaghimi, Effect of Substrate Temperature on the Properties of Coatings and Splats Deposited by Wire Arc Spraying, *Surf. Coat. Technol.*, 2006, **201**(6), p 3350-3358
35. R. Dhiman, A.G. McDonald, and S. Chandra, Predicting Splat Morphology in a Thermal Spray Process, *Surf. Coat. Technol.*, 2007, **201**(18), p 7789-7801